Influence of symmetry breaking in pentamers on Fano resonance and near-field energy localization

M. Rahmani,[1,2] B. Lukiyanchuk,[1] T. T. V. Nguyen,[3] T. Tahmasebi,[1, 2] Y. Lin,[1] T. Y. F. Liew,[1,2] and M. H. Hong[2,*]

[1]*Data Storage Institute, (A*STAR) Agency for Science Technology and Research, 5 Engineering Drive 1, Singapore 117608, Singapore*

[2]*Department of Electrical and Computer Engineering, National University of Singapore, 4 Engineering Drive 3, Singapore 117576, Singapore*

[3]*Advanced Materials for Micro- and Nano-Systems Programmed, Singapore–MIT Alliance, Singapore 117576, Singapore*

**elehmh@nus.edu.sg*

Abstract: Arrays of asymmetric pentamers are designed and fabricated with an offset of the central nano-disk position to study the effect of symmetry breaking in pentamers. It is found that while planar symmetric oligomers can exhibit a single Fano Resonance (FR), an offset of the central nano-disk at a controlled gap of 3 nm from the nearest neighbor nano-disk, gives rise to the appearance of an additional dark mode that can potentially be used in localized surface plasmon resonance sensing. It is shown that this mode leads to the appearance of the second FR in the same spectrum. The simulation results are in a good agreement with experimental data. Furthermore, it is found that unique near-field energy distribution in the asymmetric pentamers can be well tuned to be localized at one, two or three of the four subwavelength gaps of the pentamer selectively by only changing the polarization orientation of a single light source.

OCIS codes: (240.6680) Surface plasmons; (260.5740) Resonance; (230.5440) Polarization-selective devices; (250.6715) Switching.

References and links

1. W. L. Barnes, A. Dereux, and T. W. Ebbesen, "Surface plasmon subwavelength optics," Nature **424**(6950), 824–830 (2003).
2. P. K. Jain, X. Huang, I. H. El-Sayed, and M. A. El-Sayed, "Noble metals on the nanoscale: optical and photothermal properties and some applications in imaging, sensing, biology, and medicine," Acc. Chem. Res. **41**(12), 1578–1586 (2008).
3. F. Hao, P. Nordlander, Y. Sonnefraud, P. V. Dorpe, and S. A. Maier, "Tunability of subradiant dipolar and fano-type plasmon resonances in metallic ring/disk cavities: implications for nanoscale optical sensing," ACS Nano **3**(3), 643–652 (2009).
4. L. V. Brown, H. Sobhani, J. B. Lassiter, P. Nordlander, and N. J. Halas, "Heterodimers: plasmonic properties of mismatched nanoparticle pairs," ACS Nano **4**(2), 819–832 (2010).
5. A. Christ, O. J. F. Martin, Y. Ekinci, N. A. Gippius, and S. G. Tikhodeev, "Symmetry breaking in a plasmonic metamaterial at optical wavelength," Nano Lett. **8**(8), 2171–2175 (2008).
6. N. Liu, L. Langguth, T. Weiss, J. Kästel, M. Fleischhauer, T. Pfau, and H. Giessen, "Plasmonic analogue of electromagnetically induced transparency at the Drude damping limit," Nat. Mater. **8**(9), 758–762 (2009).
7. B. Lukiyanchuk, N. I. Zheludev, S. A. Maier, N. J. Halas, P. Nordlander, H. Giessen, and C. T. Chong, "The Fano resonance in plasmonic nanostructures and metamaterials," Nat. Mater. **9**(9), 707–715 (2010).
8. J. B. Lassiter, H. Sobhani, J. A. Fan, J. Kundu, F. Capasso, P. Nordlander, and N. J. Halas, "Fano resonances in plasmonic nanoclusters: geometrical and chemical tunability," Nano Lett. **10**(8), 3184–3189 (2010).
9. J. A. Fan, K. Bao, C. Wu, J. Bao, R. Bardhan, N. J. Halas, V. N. Manoharan, G. Shvets, P. Nordlander, and F. Capasso, "Fano-like interference in self-assembled plasmonic quadrumer clusters," Nano Lett. **10**(11), 4680–4685 (2010).

#155177 - $15.00 USD Received 22 Sep 2011; revised 13 Oct 2011; accepted 21 Oct 2011; published 2 Nov 2011

10. M. Rahmani, T. Tahmasebi, Y. Lin, B. Lukiyanchuk, T. Y. F. Liew, and M. H. Hong, "Influence of plasmon destructive interferences on optical properties of gold planar quadrumers," Nanotechnology **22**(24), 245204 (2011).
11. M. Rahmani, B. Lukiyanchuk, B. Ng, A. Tavakkoli K. G., Y. F. Liew, and M. H. Hong, "Generation of pronounced Fano resonances and tuning of subwavelength spatial light distribution in plasmonic pentamers," Opt. Express **19**(6), 4949–4956 (2011).
12. M. Hentschel, M. Saliba, R. Vogelgesang, H. Giessen, A. P. Alivisatos, and N. Liu, "Transition from isolated to collective modes in plasmonic oligomers," Nano Lett. **10**(7), 2721–2726 (2010).
13. M. Hentschel, D. Dregely, R. Vogelgesang, H. Giessen, and N. Liu, "Plasmonic oligomers: the role of individual particles in collective behavior," ACS Nano **5**(3), 2042–2050 (2011).
14. M. Hentschel, D. Dregely, R. Vogelgesang, H. Giessen, and N. Liu, "Plasmonic oligomers: the role of individual particles in collective behavior," ACS Nano **5**(3), 2042–2050 (2011).
15. W. Zhang, L. Huang, C. Santschi, and O. J. F. Martin, "Trapping and sensing 10 nm metal nanoparticles using plasmonic dipole antennas," Nano Lett. **10**(3), 1006–1011 (2010).
16. M. Righini, A. S. Zelenina, C. Girard, and R. Quidant, "Parallel and selective trapping in a patterned plasmonic landscape," Nat. Phys. **3**(7), 477–480 (2007).
17. W. Srituravanich, N. Fang, C. Sun, S. Durant, M. Ambati, and X. Zhang, "Plasmonic lithography," in ASME 2004 3rd Integrated Nanosystems Conference (NANO2004), Pasadena, California, USA, September 22–24, 2004, pp. 99–100, doi:10.1115/NANO2004-46023.
18. M. Aeschlimann, M. Bauer, D. Bayer, T. Brixner, F. J. García de Abajo, W. Pfeiffer, M. Rohmer, C. Spindler, and F. Steeb, "Adaptive subwavelength control of nano-optical fields," Nature **446**(7133), 301–304 (2007).
19. G. Margheri, T. Del Rosso, S. Sottini, S. Trigari, and E. Giorgetti, "All optical switches based on the coupling of surface plasmon polaritons," Opt. Express **16**(13), 9869–9883 (2008).
20. B. S. Lukiyanchuk, M. I. Tribelsky, V. Ternovsky, Z. B. Wang, M. H. Hong, L. P. Shi, and T. C. Chong, "Peculiarities of light scattering by nanoparticles and nanowires near plasmon resonance frequencies in weakly dissipating materials," J. Opt. A, Pure Appl. Opt. **9**(9), S294–S300 (2007).
21. B. S. Lukiyanchuk, M. I. Tribelsky, Z. B. Wang, Y. Zhou, M. H. Hong, L. P. Shi, and T. C. Chong, "Extraordinary scattering diagram for nanoparticles near plasmon resonance frequencies," Appl. Phys., A Mater. Sci. Process. **89**(2), 259–264 (2007).
22. M. I. Tribelsky, S. Flach, A. E. Miroshnichenko, A. V. Gorbach, and Y. S. Kivshar, "Light scattering by a finite obstacle and fano resonances," Phys. Rev. Lett. **100**(4), 043903 (2008).
23. X. R. Su, Z. S. Zhang, L. H. Zhang, Q. Q. Li, C. C. Chen, Z. J. Yang, and Q. Q. Wang, "Plasmonic interferences and optical modulations in dark-bright-dark plasmon resonators," Appl. Phys. Lett. **96**(4), 043113 (2010).

1. Introduction

Recent advancements in nano-fabrication and nano-optical characterization and improvements in full-field computational electromagnetics, have provided rich opportunities to study the near surface collective electronic oscillations known as surface plasmons [1]. Many novel optical properties of plasmonic nano-structures are a result of the interaction among plasmons arising from different individual components of the nano-structures [2,3]. Several studies have been recently undertaken to investigate the effect of the perturbations, such as symmetry breaking [4,5] and mismatched nano-particles pairs [4], which lead to a destructive interference among plasmon modes attributed to new phenomena like electromagnetically induced transparency [6] and Fano Resonance (FR) [7]. In contrast to the Lorentzian resonance, FR exhibits a distinctly asymmetric spectrum shape which is highly sensitive to many disordering factors, such as variation in geometries, dielectric environment and polarization excitation [7]. These inherent sensitivities have spurred interest in coupled symmetrical structures, which provides a higher sensitivity optical response than uncoupled plasmonic structures [8]. Recently planar symmetric oligomers, such as quadrumers [9,10], pentamers [11] and heptamers [8,12] have shown to exhibit a single FR at normal light incidence. The reason for the FR emergence in such structures is attributed to the destructive interference among the anti-parallel dipolar modes [11,13] rather than the excitation of high-order modes [8]. Hence in the planar symmetric oligomers, the pronounced FR is more readily to be achieved than asymmetric structures [10,11]. Furthermore, the effects of the disk size, geometry and local dielectric environment on the FR in some oligomers, such as heptamers, were studied as well [9]. Moreover, the effect of the symmetry breaking in the heptamers was also considered. It has been shown that the removal of one of the peripheral disks of a

#155177 - $15.00 USD Received 22 Sep 2011; revised 13 Oct 2011; accepted 21 Oct 2011; published 2 Nov 2011

heptamer can result in a shift of FR position [9], and the displacement in the central disk position can lead to the emergence of a new FR while the first FR is diminished [14].

In this work, the effect of the geometrical symmetry breaking on the optical properties of the pentamers is investigated. While it was recently shown that among oligomers, pentamers can exhibit higher contrast FR [11], the contribution of the central nano-disk of a pentamer to the FR behavior is revealed by physically offsetting its central nano-disk in this paper. It leads to a better understanding of the nature of electromagnetic coupling in pentamers which could find remarkable potential applications for localized surface plasmon resonance bio-chemical sensing. It is established with a high controlled offset of the position of the central nano-disk, for only 3 nm gap with the nearest neighbor disk. It is shown that an additional FR as well as unique spatial energy distribution appear with this disks arrangement. While these bi-FRs' spectra in the asymmetric pentamer can find potential applications in bio-chemical detection [8], the subwavelength dynamic localization of electromagnetic intensity on the nanometer scale gaps can overcome the spatial restriction of conventional optics as well. It is an extension of the optical trapping of nanoparticles at very small gaps of plasmonic dipole antennas [15] and selective trapping in a patterned plasmonic landscape [16]. As compared to the asymmetric heptamers, this selective energy distribution provides a number of potential applications in nano-lithography [17], nonlinear spectroscopy [18], optical information processing such as optical modeling and switching [19] and other research fields in which optical investigations are carried out with high spatial resolution.

2. Experimental

The nano-structures were fabricated by the electron beam lithography (Elonix 100KV EBL system) on silicon substrates with 100 nm $\mathbf{SiO_2}$ on the surface. Firstly, 3 nm thick Ti film was deposited by e-beam evaporation (EB03 BOC Edwards) on the substrates to increase the adhesion between Au and substrates. Then a 50 nm Au film was evaporated on the Ti film. Subsequently a negative resist, hydrogen silsesquioxane (HSQ), was spin coated. After exposure and development, the nano-structures on the electro-resist were transferred down to the metallic films by ion milling. In this work, three types of pentamers are designed and fabricated. To characterize the fabricated samples, UV-Vis-NIR micro-spectrophotometer (CRAIC QDI 2010 based on a Leica DMR microscope) was used for the spectrum measurement. A normally incident light with linear polarization was applied to excite the nano-structures. Simulated spectra were obtained by a three-dimensional finite-difference time domain technique (FDTD) in the wavelength range of 300 ~1000 nm.

3. Results and discussion

The designed and fabricated pentamers, accompanied by corresponding simulation and experimental reflection spectra are shown in Fig. 1. Figures 1(a)–1(c) show the SEM images of the periodic patterns of the fabricated nano-structures. The diameter and height of each individual nano-disk are 125 nm and 50 nm, respectively. Type I pentamer shown in Fig. 1(a) is the symmetric pentamer in which the central nano-disk posses equal gaps to all four surrounding disks. But Type II and Type III pentamers, shown respectively in Figs. 1(b) and 1(c), are asymmetric pentamers with an offset of the central disk position at 6 nm and 12 nm, respectively. Hence, the gaps between the central disk and other disks for Type I pentamer are 15 nm. In the Type II and Type III pentamers, the offsets of the central disk position lead to the appearance of a smaller gap between the central disk and the nearest neighbor disk at a gap size of 9 and 3 nm, respectively.

In Fig. 1(d), the Fano-line shape in the reflection spectra of Type I pentamer can be observed to be in good agreement between the simulation and characterization, apart from a small shift which is due to the absence of substrate in the simulation. As can be seen in the simulation spectrum of the Type I pentamer, the full width half maximum (FWHM) of Fano dip is around 100nm. Previous studies on symmetric pentamers [11] reveal that super-radiant

#155177 - $15.00 USD Received 22 Sep 2011; revised 13 Oct 2011; accepted 21 Oct 2011; published 2 Nov 2011

mode in the pentamers occurs when the plasmons of all the disks oscillate in phase, while the sub-radiant mode becomes apparent as the opposite anti-parallel dipolar moments appear. The Fano-line shape as the result of the existence of these two modes can be seen in the experimental reflection spectrum of the fabricated Type I pentamer at ~650 nm. It is worth mentioning that the peak position of the super-radiant mode cannot be exactly determined from the spectrum due to the presence of the resonance dip. Therefore, it can be concluded that the FR comes to existence when these opposite dipolar plasmons, arising from the individual components, lead to the destructive interference between the super-radiant and sub-radiant modes [11].

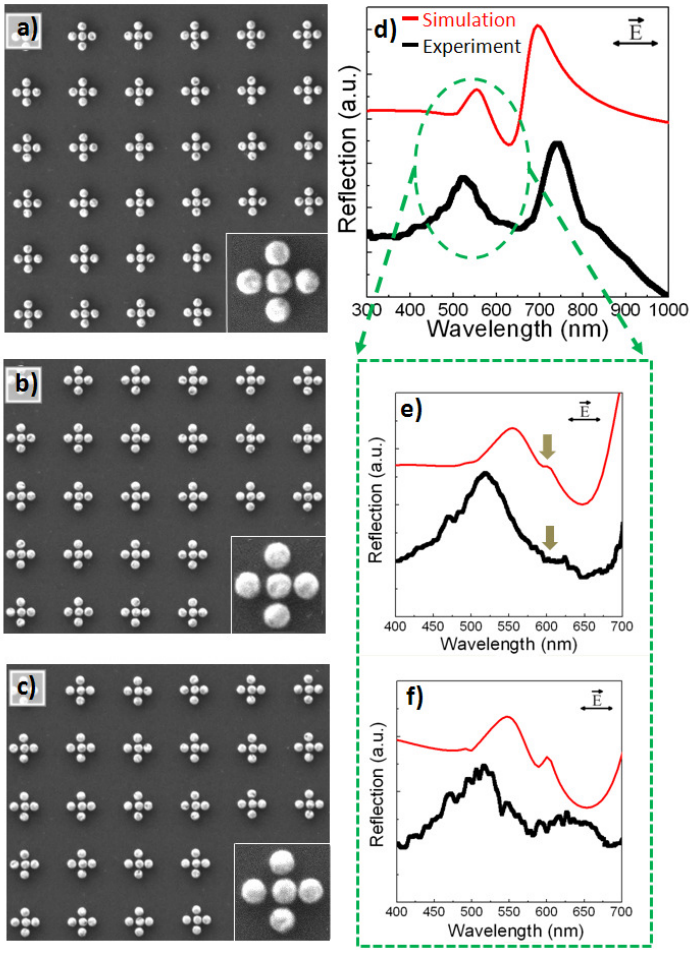

Fig. 1. SEM images of the periodic array nano-patterns of (a) Type I symmetric pentamer, (b) Type II and (c) Type III asymmetric pentamers. The offset of the central disk for the Type II and Type III asymmetric pentamers are 6 nm and 12 nm, respectively leading to a corresponding gap of 9 nm and 3 nm gaps. (d), (e) and (f) simulated and experimental reflection spectra along x-polarized normal incidence of the corresponding pentamers in (a), (b) and (c). Diameter of each disk is 125 nm.

Interestingly the second FR in the same reflection spectrum appears when an offset is applied to the central nano-disk with respect to the other four surrounding nano-disks. However, because of very small inter-particle gaps in Type II and Type III pentamers, the fabrication defects such as surface roughness and size distributions, affect the experimental measurements leading to the inevitable noise in experimental results. Figures 1(b) and 1(e)

#155177 - $15.00 USD Received 22 Sep 2011; revised 13 Oct 2011; accepted 21 Oct 2011; published 2 Nov 2011

show the SEM image of Type II pentamers and corresponding measured and simulated reflection spectra. For the better observation of the second FR, the experimental and simulation results of the reflection spectra are shown in the wavelengths from 400 to 700 nm. Small change in the reflection spectra of Type II pentamer can be observed in Fig. 1(e) at a wavelength of ~600 nm, but the second FR is more obvious in Type III pentamer, where a bigger offset of the central disk is applied. Figure 1(c) shows the SEM image of the periodic pattern Type III pentamers and Fig. 1(f) reveals the corresponding reflection spectra in which the second Fano-line shape appears at ~580nm with a FWHM of around 50 nm in simulation results.

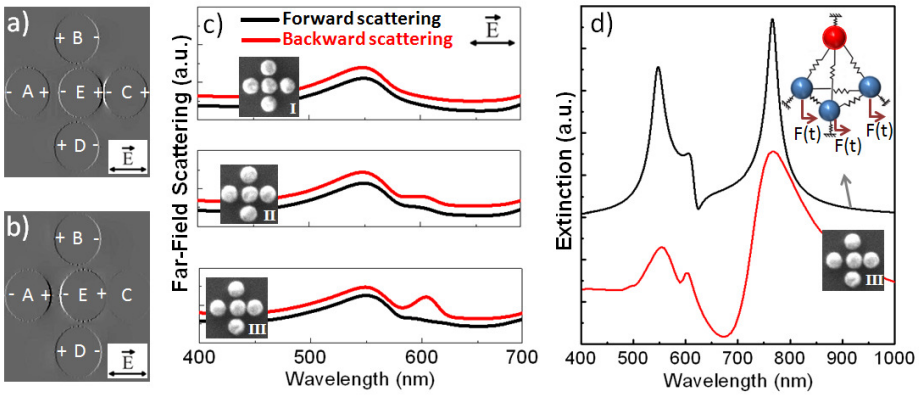

Fig. 2. Calculated charge distribution of Type III pentamer at a wavelength of (a) 650 nm (b) 580 nm. (c) Calculated forward and backward far-field scattering of Type I, II and III pentamers and (d) Simulated FDTD (red line) and oscillator model calculated (black line) extinction spectra of Type III pentamer.

In order to study the characteristics of this second FR, the charge distribution and far-field scattering spectra are calculated. Figures 2(a) and 2(b) show the charge distribution of Type III pentamer at the wavelengths of 650 nm and 580 nm, respectively. 650 nm is the wavelength in which the condition of the significant destructive interference between the sub-radiant and super-radiant modes is sufficiently fulfilled and subsequently the first FR occurs. The charge distribution shown in Fig. 2(a) reveals that compared to the symmetric pentamer [11], the Type III pentamer exhibits net anti-parallel collective dipole modes at ~650 nm, as long as the gap among disks exists. This plot shows the configuration of these anti-parallel modes of disks A, E and C oscillate in the opposite phase with respect to disks B and D. The ratio between the opposing phase oscillating plasmons is kept as a constant of 2/3 [11]. Figure 2(b) shows the charge distribution of Type III pentamer at the wavelength of 580 nm. As the plot reveals, in this wavelength the charges inside the disk C are not well distributed with respect to the other disks, although the gap between disks C and E is much smaller than the gap between disks A and E. Meanwhile, disks B and D still exhibit dipolar charge distribution similar to the first FR charge distribution pattern. The charge density plotted in Fig. 2(b) is comparable with recently investigated quadrumers [9], in which Fano-like interference was characterized by the narrow dip in the scattering spectrum due to the anti-parallel dipoles. In this case, the Fano minimum shows only the dark mode, which leads to resonant energy storage in this mode and suppression of the bright mode. It can be seen from Fig. 2(b) that the net dipole moment of the pentamer unit cell is small because the dipoles of the disks A and E are oriented oppositely to the disks B and D. As a result, the scattered fields from the pentamer interfere destructively and the mode becomes sub-radiant. As shown previously in Fig. 2(a), the super-radiant mode in the pentamer totally disappears when reflection spectrum experiences its dip [8,11,12] at ~650 nm. In other words, all disks in the pentamer should

#155177 - $15.00 USD Received 22 Sep 2011; revised 13 Oct 2011; accepted 21 Oct 2011; published 2 Nov 2011

experience a net mixture of both sub-radiant and super-radiant modes at 580 nm. But as a result of symmetry breaking in pentamers, the new dark sub-radiant mode happens among this mixture of sub-radiant and super-radiant modes, leading to the appearance of the second FR.

It is well known that the dark mode exhibits extremely high sensitivity to the incident light, where small variations in its wavelength can change far-field forward and backward scattering spectra differently [20,21]. Figure 2(c) shows the calculated far-field backward and forward scattering profiles for Types I, II and III pentamers, respectively which can be explained by using the Mie solution [22]. The spectra were calculated at precisely 0 and 180 degrees with respect to the wave vector which is perpendicular to the substrate. After applying the offset of the central disk position, the backward far-field scattering is amplified while the forward far-field scattering does not experience a big difference. This trend can be observed clearly in the far-field scattering spectrum from 580 nm to 650 nm, where the symmetry breaking leads to an additional interference between the forward and the backward scattering [20,21]. The effect of the offset induces a small change in the forward and backward scattering spectra at the wavelength of 580 nm for Type II pentamer and subsequently more obvious for Type III pentamer where, upon to the symmetry breaking, new sub-radiant mode gives rise to the second Fano interference at ~580 nm. Keeping in mind that symmetry breaking in pentamers leads to the emergence of the second FR only with x-polarized light and the optical properties of asymmetric pentamers are polarization-dependent unlike the symmetric pentamers which are polarization-independent [11].

An analogous of the optical responses to the mass-spring model is one more way to prove the existence of the second FR in plasmonic systems. Figure 2(d) shows the comparison between the extinction spectrum of pentamer Type III, simulated by Lumerical FDTD at x-polarized normal incidence and the power extinction of the oscillator system calculated by the motion equations of 4 coupled interacting oscillator model. This model is a simplified model of the spring-mass model consisting of five coupled interacting oscillators, which can reproduce the optical responses of the pentamer Type III. The simplified 3 coupled interacting oscillators model has been used to demonstrate the emergence of the first FR in symmetric pentamers recently [11]. The similar coupling among disks A and C with respect to disk E, as well as disks B and D with respect to disk E in symmetric pentamers, allowed that system to be simplified from 5 oscillators to 3 oscillators [11]. But in Type II and III pentamers, the coupling among disks A and C with respect to disk E are different because of different inter-disk distances. However the interaction among disks B and D with respect to disk E are still similar. Thus 4 interacting oscillators are established from the mass-spring modeling. In this system, 3 blue oscillators represent 4 outer disks in analogous asymmetric pentamers and red oscillator represents the central disk. Since the surrounding disks are responsible for bright mode exhibition in such optical systems, all blue oscillators are driven by harmonic force $\mathbf{F}(t)$. The good agreement between mass-spring calculated and FDTD simulated extinction spectra shown in Fig. 2(d) demonstrates clearly hybridized plasmon modes attributing to twin FRs appearance in both systems.

More interestingly, there is an unique capability for Type III pentamer to localize the near-field energy selectively. It is found that the polarization orientation can flexibly tune the localization of the near-field energy. Figure 3 shows the calculated near-field energy intensity distribution in Type III pentamer at the normal incidence of a single light source at the wavelength of 700 nm for various polarizations. Figure 3(a) shows that when the structure is illuminated by the x-polarized light, energy localization can be achieved in the 3 nm gap between the central disk E and disk C, while the interaction between the central disk C and disk A experiences the minimum amount of the stored energy at this wavelength. Figure 3(b) shows the effect of the y-polarized light on the localization of the energy. In this case, all the energy is stored at the gaps among the central disk E and disks B and D. An interesting feature appears when the light polarization is changed to 45 degree with respect to the x-axis in the xy plane. As can be seen in Fig. 3(c), the near-field energy is unequally distributed among three

#155177 - $15.00 USD Received 22 Sep 2011; revised 13 Oct 2011; accepted 21 Oct 2011; published 2 Nov 2011

gaps of the central disk E and disks B, C and D. While the two gaps among the central disk E and the disks B and D, store equal near-field energy, the gap between central disk E and disk C exhibits a higher amount of localized energy. These selective energy localizations show the advantages of Type III pentamer as compared to the symmetric pentamers [11], in which the near-field energy can be tuned either along x- or y-direction, selectively. This ability can also be an advantage as compared to the optical trapping of Au nanoparticles within 10 nm inter-particle gap of plasmonic dipole antennas [15], where the electric field can be localized in the nano-gap leading to a field enhancement. However, the structures` polarization sensitivity in this work is theoretically analyzed while it has been shown that nano-particle trapping can be recorded in real time by monitoring the Rayleigh scattering spectra of individual plasmonic antennas [15]. This polarization sensitivity can be applied in non-linear spectroscopy [21], and optical modulation such as switches [22]. Figure 3 also shows that the tuning of spatial near-field localization in the asymmetric pentamers can be established without the requirement of co-illumination by two light sources [23] or the adjustment of the phase delay between them [18].

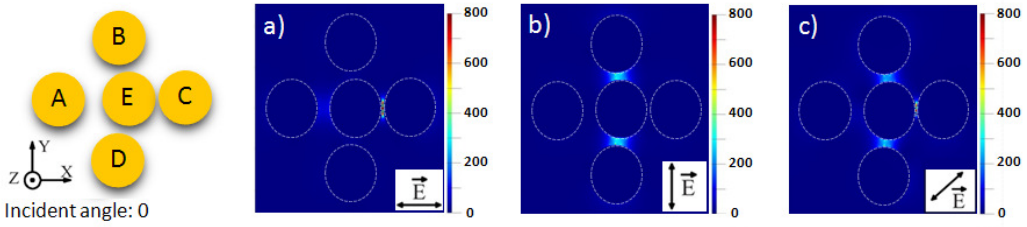

Fig. 3. Calculated near-field energy distribution within the Type III pentamer at x-polarized normal incidence and a wavelength of 700 nm: (a) x- polarization, (b) y-polarization and (c) 45-degree polarization, with respect to x axis.

4. Conclusions

In summary, it is investigated that by applying an offset to the central disk in pentamers, new sets of optical characteristics can be observed. It is found that in the asymetric pentamers, an additional FR occurs while the first FR exists. The measured distinct spectral features in high-quality fabricated nano-structures at a precisely controlled gap down to 3 nm are in good agreement with the simulation. Furthermore, it is theoretically investigated that once an additional dark mode in the unit cell of the pentamer appears, how the change in far-field forward and backward scattering behavior, atteributes to the second FR emergence. Only changing the polarization orientation of a single light source in the assymetric pentamer has unique potential to tune the localization of the near-field energy at the gaps inside the pentamer selectively and can be used as a versatile tool for optical trapping.

Acknowledgments

The authors would like to acknowledge the funding provided by SERC Agency of Science, Technology And Research (A*STAR) Superlens Program (Project No. 092 154 0099). Mohsen Rahmani would like to express his gratitude for the support from the A*STAR–SINGA program.

#155177 - $15.00 USD Received 22 Sep 2011; revised 13 Oct 2011; accepted 21 Oct 2011; published 2 Nov 2011